Monthly Notices
of the
ROYAL ASTRONOMICAL SOCIETY
MNRAS **443,** 678–686 (2014) doi:10.1093/mnras/stu1240

The X-ray spectra of the first galaxies: 21 cm signatures

Fabio Pacucci,[1⋆] Andrei Mesinger,[1] Stefano Mineo[2] and Andrea Ferrara[1,3]

[1]*Scuola Normale Superiore, Piazza dei Cavalieri, 7 I-56126 Pisa, Italy*
[2]*Harvard–Smithsonian Center for Astrophysics, 60 Garden Street Cambridge, MA 02138, USA*
[3]*Kavli Institute for the Physics and Mathematics of the Universe (WPI), Todai Institutes for Advanced Study, the University of Tokyo, Kashiwa, Chiba 277-8583, Japan*

Accepted 2014 June 20. Received 2014 June 10; in original form 2014 March 20

ABSTRACT

The cosmological 21 cm signal is a physics-rich probe of the early Universe, encoding information about both the ionization and the thermal history of the intergalactic medium (IGM). The latter is likely governed by X-rays from star formation processes inside very high redshift ($z \gtrsim 15$) galaxies. Due to the strong dependence of the mean free path on the photon energy, the X-ray spectral energy distribution (SED) can have a significant impact on the interferometric signal from the cosmic dawn. Recent *Chandra* observations of nearby, star-forming galaxies show that their SEDs are more complicated than is usually assumed in 21 cm studies. In particular, these galaxies have ubiquitous, sub-keV thermal emission from the hot interstellar medium (ISM), which generally dominates the soft X-ray luminosity (with energies $\lesssim$1 keV, sufficiently low to significantly interact with the IGM). Using illustrative soft and hard SEDs, we show that the IGM temperature fluctuations in the early Universe would be substantially increased if the X-ray spectra of the first galaxies were dominated by the hot ISM, compared with X-ray binaries with harder spectra. The associated large-scale power of the 21 cm signal would be higher by a factor of $\sim$3. More generally, we show that the peak in the redshift evolution of the large-scale ($k \sim 0.2$ Mpc^{-1}) 21 cm power is a robust probe of the soft-band SED of the first galaxies, and importantly, is not degenerate with their bolometric luminosities. On the other hand, the redshift of the peak constrains the X-ray luminosity and halo masses which host the first galaxies.

Key words: galaxies: high-redshift – cosmology: theory – X-rays: binaries – X-rays: diffuse background – X-rays: galaxies – X-rays: ISM.

1 INTRODUCTION

The redshifted 21 cm line is sensitive to the thermal and ionization state of the cosmic gas, making it a powerful probe of the early Universe. As it is a line transition, it has the potential to map out the 3D structure of cosmic gas and its evolution. First generation interferometers, including the Low Frequency Array van Haarlem et al. 2013),[1] Murchison Wide Field Array (MWA; Tingay et al. 2013),[2] and the Precision Array for Probing the Epoch of Reionization (PAPER; Parsons et al. 2010),[3] are already taking data. Their focus is on a statistical detection of reionization, though even earlier epochs of heating (when the cosmic gas was heated to temperatures above the cosmic microwave background, CMB) could be detectable (Mesinger, Ewall-Wice & Hewitt 2014). Second generation instruments, like the Square Kilometre Array (SKA; Mellema et al. 2013)[4] will be coming on-line soon, with high sensitivity and wide frequency coverage, allowing us to witness the birth of the very first galaxies through their imprint on the intergalactic medium (IGM).

X-rays play a very important role during these epochs. Reionization with a significant X-ray contribution proceeds more uniformly, complicating the interpretation of 21 cm fluctuations on large scales (Mesinger, Ferrara & Spiegel 2013). More importantly, X-rays are thought to be responsible for heating the IGM to temperatures above the CMB, before reionization gets well underway (e.g. Furlanetto 2006; McQuinn & O'Leary 2012). In fiducial models, the large-scale temperature fluctuations during this heating epoch are responsible for the strongest 21 cm interferometric signal, an order of magnitude greater than the signal during reionization. Understanding the timing and homogeneity of X-ray

⋆E-mail: fabio.pacucci@sns.it
[1] http://www.lofar.org/
[2] http://www.mwatelescope.org/
[3] http://eor.berkeley.edu
[4] http://www.skatelescope.org/

heating is critical in interpreting 21 cm observations of the pre-reionization and reionization epochs (e.g. Pritchard & Furlanetto 2007; Mesinger et al. 2014).

A common approach is to parametrize our uncertainty of the early X-ray background (XRB) by fixing the galactic X-ray spectral energy distribution (SED), and varying its normalization, i.e. bolometric luminosity (e.g. Furlanetto 2006; Santos et al. 2011; Christian & Loeb 2013; Mesinger et al. 2014; though see also exploratory work in Pritchard & Furlanetto 2007; Baek et al. 2010; Mesinger et al. 2013). The X-ray luminosity of the first galaxies[5] regulates the timing of the heating epoch. However, the actual X-ray SED should also be important in setting the signal, as the mean free path of X-rays through the IGM, λ_X, has a very strong dependence on the photon energy (e.g. Furlanetto, Oh & Briggs 2006; McQuinn 2012):

$$\lambda_X \approx 34\ \bar{x}_{H\,I}^{-1} \left(\frac{E_X}{0.5\ \mathrm{keV}}\right)^{2.6} \left(\frac{1+z}{15}\right)^{-2} \text{comoving Mpc}, \quad (1)$$

where $\bar{x}_{H\,I}$ is the mean neutral fraction of the IGM. Soft photons are much more likely to be absorbed closer to the galaxies, while high-energy photons heat (or ionize) the IGM more uniformly. Indeed, Mesinger et al. (2013) showed that if X-ray heating is dominated by high-energy photons, the redshift evolution of the amplitude of the large-scale 21 cm power spectrum does not show an associated pronounced peak. It is important to also note that because of this strong energy dependence of λ_X, photons with energies $\gtrsim$2 keV effectively free-steam, barely interacting with the IGM; this makes the soft X-ray SED much more relevant for the 21 cm signal.

Observations show that the SED of local galaxies is more complicated than is usually assumed in 21 cm studies. Locally, the hot interstellar medium (ISM) contributes significantly to the galaxy's soft X-ray emission (e.g. Strickland et al. 2000, 2004; Grimes et al. 2005; Owen & Warwick 2009; Li & Wang 2013; see the review in section 7.1 of Mineo, Gilfanov & Sunyaev 2012b). As an example, we note that using *Chandra*, Mineo et al. (2012b) recently studied the diffuse emission in a local sample of 21 star-forming galaxies, finding sub-keV thermal emission from the hot ISM in *every* galaxy in the sample. The stacked, bolometric soft-band (0.5–2 keV) luminosity per star formation rate (SFR) of the thermal emission is comparable to that from resolved sources, dominated by high-mass X-ray binaries (HMXBs) with much harder spectra (e.g. Gilfanov, Grimm & Sunyaev 2004; Mineo, Gilfanov & Sunyaev 2012a).

In this paper, we illustrate the impact of the X-ray SED of the first galaxies on the 21 cm power spectrum. We use simple models representative of dominant populations of either soft (corresponding to the hot ISM) or hard (corresponding to HMXBs) X-ray sources. To show the robustness of our results, we also vary the X-ray luminosity per SFR (SED normalization) and the halo mass which hosts the dominant galaxy population.

As this work was nearing completion, a related study was published by Fialkov, Barkana & Visbal (2014). The most important distinction between the two works is that our analysis is motivated by *Chandra* observations of nearby star-forming galaxies, rather than a theoretical model of HMXBs. Furthermore, our proof-of-concept focuses on predicting qualitative trends which are robust to the many astrophysical uncertainties.

This paper is organized as follows. In Section 2, we discuss possible contributions to the X-ray SED of high-z galaxies, placing them in the context of recent *Chandra* observations. In Section 3, we present our simulations of the cosmological 21 cm signal. In Section 4, we discuss our main results, showing how the SED has a robust imprint in the 21 cm signal. Finally, we conclude in Section 5. Unless stated otherwise, we quote all quantities in comoving units. Throughout, we adopt recent Planck cosmological parameters (Planck Collaboration 2013): $(\Omega_m, \Omega_\Lambda, \Omega_b, h, n_s, \sigma_8) = (0.32, 0.68, 0.049, 0.67, 0.96, 0.83)$.

2 X-RAYS FROM THE FIRST GALAXIES

As we do not know the X-ray SEDs of high-redshift, $z > 10$, galaxies[6] we are forced to make educated guesses, motivated by observations of low-z ($z \lesssim 4$) galaxies. In the local Universe, active galactic nuclei (AGN) dominate the XRB (e.g. Moretti et al. 2012). However, at high-redshifts ($z \gtrsim 5$; e.g. Haardt & Madau 2012; Fragos et al. 2013), the contribution of AGN to the XRB should become subdominant to that of end products of stellar evolution, accreting gas from companion stars. These are characterized by the masses of their donor stars, and comprise HMXBs, intermediate-mass X-ray binaries, low-mass X-ray binaries (LMXBs), cataclysmic variables and active binaries. However, the characteristic time-scales of all but the HMXBs are longer than the Hubble time at the very high redshifts of interest. Furthermore, the bolometric[7] X-ray luminosity of local, star-forming galaxies is found to be dominated by resolved HMXBs (e.g. Grimm, Gilfanov & Sunyaev 2003; Ranalli, Comastri & Setti 2003; Swartz et al. 2004; Persic & Rephaeli 2007; Lehmer et al. 2010; Swartz et al. 2011; Walton et al. 2011; Mineo et al. 2012a). For these reasons, many studies of early IGM heating focus on HMXBs as the primary source of X-rays in star-forming galaxies (e.g. Furlanetto 2006; Pritchard & Furlanetto 2007; Mesinger, Furlanetto & Cen 2011; Santos et al. 2011; though see e.g. Valdés et al. 2013; Evoli et al., in preparation for more exotic models in which heating can be dominated by annihilating dark matter).

On the other hand, the hot ISM could contribute a significant amount of soft X-rays. Heated by supernovae explosions and winds to temperatures of 10^{6-7} K, this hot plasma emits X-rays through a combination of thermal bremsstrahlung and metal line cooling. It is diffuse and more spatially extended than the point sources discussed above. Its presence is typically detected in normal star-forming galaxies and starbursts (e.g. Strickland et al. 2000, 2004; Grimes et al. 2005; Mineo et al. 2012b; Li & Wang 2013), as well as in high-resolution ISM simulations of the first, atomically cooled galaxies (e.g. Wise et al. 2012; Aykutalp et al., in preparation). The contribution of soft emission from the hot ISM to the X-ray heating epoch has not been considered previously.

Below we take HMXBs and the hot ISM as the two potential sources of X-ray emission from the first galaxies. In nearby

[5] For convenience, we use the adjective 'first' somewhat imprecisely, referring to the galaxies responsible for heating the IGM, which likely occurs at $z \sim$ 10–20 (see below). The very first galaxies could appear even earlier ($z \sim 30$), though star formation inside these rare minihaloes is likely insufficient to significantly heat the IGM (e.g. McQuinn & O'Leary 2012). Nevertheless, our qualitative conclusions are not affected by the precise redshift at which the relevant galaxies appear (see below).

[6] QSOs at $z \lesssim 6$ have been detected in X-rays (e.g. Brandt et al. 1999; Fan et al. 1999), as well as galaxies at $z \lesssim 4$ through stacking analysis (Basu-Zych et al. 2013).

[7] We stress again that high-energy X-rays are unlikely to interact with the IGM at redshift relevant for the 21 cm signal, given their long mean free paths. Hence the soft-band ($\lesssim$2 keV) SED and luminosity is more relevant for predicting the 21 cm signal.

galaxies, the total luminosity of both of these sources is observed to be proportional to the galaxy's SFR (e.g. Gilfanov et al. 2004). Interestingly, *both HMXBs and the hot ISM have a comparable, observed soft-band (0.5–2 keV) luminosity per SFR*: ∼8 and 5 × 10^{38} erg s^{-1} $M_{\odot}$ yr^{-1}, respectively (Mineo et al. 2012a,b). However, *their SEDs are dramatically different*, as we discuss further below. We also make the distinction between the *intrinsic* and *observed (or emerging)* SEDs, the latter including absorption from the host galaxy.

2.1 The intrinsic SED of the hot, diffuse ISM

Star-forming galaxies are known to output abundant X-ray emission from hot ionized gas of sub-keV temperatures, whose luminosity correlates with the SFR of the host galaxy (e.g. Strickland et al. 2000, 2004; Grimes et al. 2005; Li & Wang 2013). Recently, Mineo et al. (2012b) presented *Chandra* observations of 21 local, star-forming galaxies, isolating the contribution of hot, diffuse ISM. They took special care of various systematic effects and controlled the contamination of unresolved emission by bright compact sources of all types as well as by unresolved faint HMXBs. Every galaxy in their sample showed evidence of hot plasma, with temperatures in the range of 0.2–0.3 keV, with 1/3 of their sample showing evidence of a second thermal peak at ∼0.7 keV.

In Fig. 1, we show the composite SED of the unresolved emission from their sample of 21 galaxies, corrected for the *Chandra* instrument response (black points). At these temperatures the emission from the hot plasma should be governed by metal line cooling and thermal bremsstrahlung (e.g. Gaetz & Salpeter 1983). At soft energies ($\lesssim$2 keV), the composite can be roughly approximated by either templates: (i) a solar-metallicity, thermal (MEKAL from XSPEC) component with mean energy $\langle kT \rangle \sim 0.3$ keV; or (ii) thermal bremsstrahlung, also with $\langle kT \rangle \sim 0.3$ keV. The latter is shown with the green dashed curve in Fig. 1. At higher energies ($\gtrsim$ 2 keV), the composite SED of the unresolved emission is dominated by faint point sources with harder spectra.

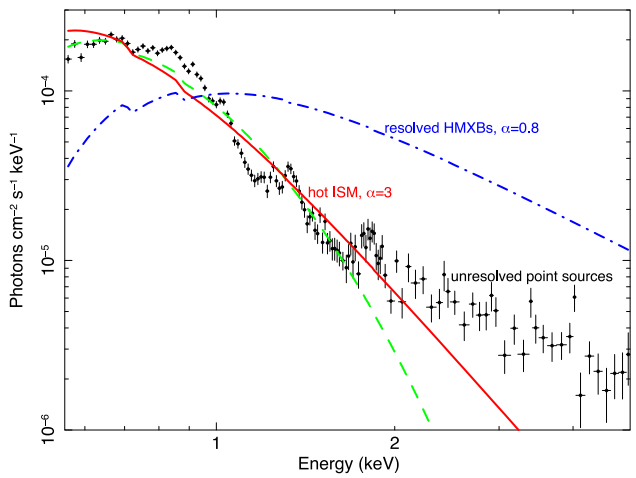

Figure 1. Composite observed X-ray SEDs from a sample of 21 local, star-forming galaxies (for further details, see Mineo et al. 2012b). Points correspond to unresolved emission, which at low energies ($\lesssim$2 keV) is dominated by the hot ISM, while at high energies ($\gtrsim$2 keV) by faint point sources (unresolved HMXBs, LMXBs, cataclysmic variables and active binaries). A best-fitting thermal bremsstrahlung profile for the hot ISM is shown with the green, dashed curve. Our fiducial toy model SED for the hot ISM (a power law with energy index $\alpha = 3$) is indicated with a solid red curve, which is a good match to the bremsstrahlung profile. The intrinsic SED for resolved HMXBs (blue dot–dashed curve) is instead a power law with energy index $\alpha = 0.8$, based on the average spectrum of HMXBs (see Swartz et al. 2004; Mineo et al. 2012a). The normalization of the blue dot–dashed curve is done to preserve the observed relative ratio of the soft-band (0.5–2 keV) luminosities per unit SFR for the HMXB and hot ISM (Mineo et al. 2012a,b). The red (blue) curve corresponds to our fiducial soft (hard) model for the intrinsic emission. In order to compare to the observed emergent spectra, all curves include intrinsic absorption by an equivalent H I column density of $N_{\rm H\,I} \sim$2–3 × 10^{21} cm^{-2}, assuming solar abundances and metallicity.

With the red solid curve we also show in Fig. 1 a power-law SED, with the specific luminosity scaling as $L_{\rm X} \propto E_{\rm X}^{\alpha}$ and an energy index of $\alpha = 3$. In our analysis below, we adopt this simple power law for the intrinsic emission for our fiducial soft SED, as it provides a reasonable fit to the SED of the hot, diffuse ISM.

2.2 The intrinsic SED of HMXBs

Composite SEDs of HMXBs generally follow a hard power law, with a spectral energy index of $\alpha \approx 0.7$–1 (Rephaeli, Gruber & Persic 1995; Swartz et al. 2004; Mineo, Gilfanov & Sunyaev 2012a). This corresponds to the so-called hard state resulting from Comptonization of soft photons on hot electrons ('corona'), in the vicinity of the compact object. Accreting compact objects also show evidence of a 'soft state', which is believed to originate in the optically thick/geometrically thin accretion disc (Shakura & Sunyaev 1973), well represented by a superposition of blackbody spectra with $\langle kT \rangle \lesssim 1$ keV (for a review see McClintock & Remillard 2006; Gilfanov 2010). However, the composite SEDs of *bright* X-ray compact sources associated with young stellar populations, such as resolved HMXBs (Mineo et al. 2012a) or ultraluminous X-ray sources (Swartz et al. 2004) are typically dominated by the 'hard state' and are well fitted with an absorbed power law (with spectral energy index of ∼0.7–1).[8]

For our fiducial hard SED below, corresponding to the intrinsic emission from bright HMXBs, we adopt a power law with energy index $\alpha = 0.8$. We show this hard power law as a blue dot–dashed curve in Fig. 1, obscured with an equivalent H I column density of $N_{\rm H\,I} \sim 3 \times 10^{21}$ cm^{-2} (Mineo et al. 2012a).

2.3 Intrinsic absorption from the host galaxy

The shape of the spectrum at low energies can depend strongly on the intrinsic absorption of the host galaxy. For our purposes, it is useful to decompose the intrinsic absorption into two contributions: (i) an H I column density and (ii) metal abundance.

For gas with a solar abundance and metallicity, the metals dominate the absorption of photons with energies $\gtrsim$0.5 keV, while helium dominates at lower energies (Morrison & McCammon 1983). The standard approach in X-ray studies is to assume a solar abundance and metallicity when constructing the absorption profile, and then quote the associated H I column density ($N_{\rm H\,I} \sim$ 2–3 × 10^{21} cm^{-2} in the case of the curves shown in Fig. 1). However, the early galaxies

[8] There is evidence that bright UXLs have a spectral cut-off at high energies, $E_{\rm X} \gtrsim$ 6–10 keV (e.g. Miyawaki et al. 2009; Bachetti et al. 2013). Our results are not sensitive to such modifications of the fiducial SED, since photons with energies above $E_{\rm X} \gtrsim 1.8 \bar{x}_{\rm H\,I}^{1/3} [(1+z)/15]^{1/2}$ keV have mean free paths exceeding the Hubble length (e.g. McQuinn 2012), and thus do not interact significantly with the IGM. However, fiducial normalizations of the X-ray luminosity to SFR ratios (see below), as well as estimates of their redshift evolution, should account for possible high-energy cut-offs (e.g. Kaaret 2014).

at $z \sim 10$–20 which drive the IGM heating should be much less enriched than local ones. If the average sightline out of the galaxy contains less metals, more soft photons would escape into the IGM for a given H I column density. Just based on qualitative arguments about metal evolution, one would expect the emergent spectra of the first galaxies to be softer than shown in Fig. 1.

It is even less clear how to estimate the H I column density of the first galaxies. Empirical trends suggest that the fraction of ionizing photons escaping galaxies increases rapidly towards high redshifts (e.g. Haardt & Madau 2012; Kuhlen & Faucher-Giguere 2012), perhaps driven by the shallower potential wells of typical galaxies which make the gas distribution more susceptible to feedback (e.g. Alvarez, Finlator & Trenti 2012; Ferrara & Loeb 2012). If confirmed, it would be reasonable to assume that the average column density relevant for X-ray absorption follows similar qualitative trends.

There could also be a relative difference in opacities for our two sources of X-rays: hot ISM and HMXBs. One could imagine that the diffuse, spatially extended hot ISM might have lower covering fractions of H I, compared to the HMXBs which can be embedded in dust clouds (which further attenuate soft X-rays). Indeed, observations of the diffuse, hot ISM show that less than half of local, star-forming galaxies have evidence of *any* host-galaxy absorption (Mineo et al. 2012b).

The discussion above is clearly very speculative, and depends on the unknown morphology and enrichment of the first galaxies. The absorption of X-ray photons by the high-z host galaxies could have a strong impact on the emerging X-ray SED, and we will return to this in future work. For this proof-of-concept, we assume a very simple model for host-galaxy obscuration, truncating the intrinsic SED at energies below <0.3 keV. Photons below this energy have an optical depth greater than unity, for the column densities greater than $N_{\rm H\,I} \gtrsim 10^{21.5}\,{\rm cm}^{-2}$, assuming that helium dominates the total opacity.[9] In other words, we assume that the first galaxies have similar column densities as local ones, but take the gas to have a low metal abundance. For illustration, we also present an 'extreme' model in which we truncate all photons with energies below $\leq$1 keV. This model is 'extreme' in the sense that it assumes that the first galaxies were much more obscured than even the more massive, evolved local ones (Fig. 1).

2.4 Normalizations of the model SEDs

Following previous work, we normalize our fiducial soft and hard SEDs with the parameter, $f_{\rm X} \equiv N_{\rm X}/0.1$, where $N_{\rm X}$ is the total number of X-ray photons escaping the galaxy per stellar baryon. For both our soft and hard spectra, the fiducial choice of $f_{\rm X} = 1$ yields band-integrated luminosities per unit SFR comparable to observed ones. Our hard SED yields a 0.5–8 keV luminosity of $L^{\alpha=0.8}_{\rm X,0.5-8keV} \approx 5 \times 10^{39}\,{\rm erg\,s^{-1}\ M_\odot\,yr^{-1}}$, similar to the observed value of $L^{\rm obs,HMXB}_{\rm X,0.5-8keV} \approx 3 \times 10^{39}\,{\rm erg\,s^{-1}\,M_\odot\,yr^{-1}}$ from equation (39) in Mineo et al. (2012a). Similarly, our soft SED yields a 0.5–2 keV luminosity of $L^{\alpha=3}_{\rm X,0.5-2\,keV} \approx 8 \times 10^{38}\,{\rm erg\,s^{-1}\ M_\odot\,yr^{-1}}$, similar to the observed value of $L^{\rm obs,ISM}_{\rm X,0.5-2\,keV} \approx 5 \times 10^{38}\,{\rm erg\,s^{-1}\,M_\odot\,yr^{-1}}$ from equation (2) in Mineo et al. (2012b).

[9] We caution that metal abundance and column density are not disentangled in present analysis of local galaxies, which assumes solar abundances and metallicity. If the sightline-averaged metallicity of the host galaxy is lower, the best-fitting H I column density would be higher, and vice versa.

We caution however that these comparisons are only illustrative. Moreover, it is difficult to guess how the relevant $z \sim 15$ galaxies are different than local ones. Using stacked spectra, Basu-Zych et al. (2013) recently measured an evolution in the X-ray luminosity to SFR ratio for star-forming galaxies out to $z \sim 4$. On the theoretical side, there is also no reason to think that the first galaxies should have similar X-ray luminosities per SFR as local ones. For example, the expected lower metallicity of early galaxies, discussed above in the context of intrinsic obscuration, could also result in a higher fraction of HMXBs (e.g. Mirabel et al. 2011; Fragos et al. 2013). Similarly, at these high redshifts Compton cooling might become important for the hot plasma (provided a large fraction of it manages to be blown out to low densities), thereby decreasing the fraction of its energy radiated away as soft X-rays. For Compton cooling to be more efficient than radiative cooling, the hot ISM (with $T \sim 10^6$ K) needs to be at densities lower than: $\lesssim 10^{-3}$–$10^{-2}\,{\rm cm^{-3}}\,[(1+z)/15]^4$, with the quoted range spanning solar to zero metallicities (e.g. Gaetz & Salpeter 1983). Modelling the ISM at these redshifts is very difficult, and model dependent. We note that numerical simulations of $T_{\rm vir} \approx 10^4$ K galaxies at $z \sim 9$–15 do find significant reservoirs of hot ISM at higher number densities (e.g. Wise et al. 2012; Aykutalp et al., in preparation), suggesting that radiative cooling would still dominate. We postpone more detailed estimates to future work. Below we explore a wide range of $f_{\rm X}$ values.

To summarize, we have two fiducial models for the X-ray spectra of the first galaxies (cf. the red and blue curves in Fig. 1): (i) a *hard* SED with a power-law index of $\alpha = 0.8$, representing X-ray emission dominated by HMXBs; and (ii) a *soft* SED with a power-law index of $\alpha = 3$, representing X-ray emission dominated by the hot ISM. In both cases, *metal-poor* gas inside the host galaxies is assumed to absorb all photons with energies below $E_0 = h\nu_0 = 0.3$ keV, corresponding to equivalent column densities as seen locally. Finally, both SEDs are normalized according to their total number of X-ray photons escaping the galaxy per stellar baryon, with the fiducial choice being $f_{\rm X} \equiv N_{\rm X}/0.1 = 1$.

It is interesting to note that the combined observed SED from both components (hot ISM + HMXBs) in local galaxies strongly resembles our fiducial, $f_{\rm X} = 1$, hard ($\alpha = 0.8$) SED for the first galaxies (see the red+blue curves in Fig. 1). This is because the absorption of the hard HMXB power law by a metal-enriched ISM is almost exactly compensated for by the absorbed soft contribution from the hot ISM. The resulting total emergent spectrum (in which the hot ISM and HMXBs comparably contribute to the soft-band luminosity per SFR) resembles an *unabsorbed*, $\alpha \sim 1$ power law down to low energies.

3 SIMULATING THE 21 cm SIGNAL

The 21 cm signal is usually represented in terms of the offset of the 21 cm brightness temperature from the CMB temperature, T_γ, at an observed frequency ν (Furlanetto et al. 2006):

$$\delta T_b(\nu) = \frac{T_{\rm S} - T_\gamma}{1+z}(1 - e^{-\tau_{\nu_{21}}})$$
$$\approx 27 x_{\rm H\,I}(1+\delta_{\rm nl}) \left(\frac{H}{{\rm d}v_r/{\rm d}r + H}\right)\left(1 - \frac{T_\gamma}{T_{\rm S}}\right)$$
$$\times \left(\frac{1+z}{10}\frac{0.15}{\Omega_{\rm M}h^2}\right)^{1/2}\left(\frac{\Omega_{\rm b}h^2}{0.023}\right){\rm mK}, \quad (2)$$

where $T_{\rm S}$ is the gas spin temperature, $\tau_{\nu_{21}}$ is the optical depth at the 21 cm frequency ν_{21}, $\delta_{\rm nl}(\boldsymbol{x}, z) \equiv (\rho/\bar{\rho} - 1)$ is the evolved

(Eulerian) density contrast, $H(z)$ is the Hubble parameter, $\mathrm{d}v_r/\mathrm{d}r$ is the comoving gradient of the line of sight component of the comoving velocity, and all quantities are evaluated at redshift $z = \nu_{21}/\nu - 1$.

To simulate the 21 cm signal, we use a parallelized version of the publicly available 21CMFAST[10] code. It uses perturbation theory and excursion-set formalism to generate density, velocity, source, ionization, and spin temperature fields. For further details and tests of the code, interested readers are encouraged to see Mesinger & Furlanetto (2007), Mesinger et al. (2011), and Zahn et al. (2011). Here we outline our simulation set-up.

Our simulation boxes are 750 Mpc on a side, with a resolution of 500^3. Density fields are generated by perturbing Gaussian initial conditions, sampled on a higher resolution, 2000^3 grid (Zel'Dovich 1970). Ionization by UV photons is computed in an excursion-set fashion, by comparing the time-integrated number of ionizing photons to the number of neutral atoms in regions of decreasing scale (Furlanetto, Zaldarriaga & Hernquist 2004). Specifically, a simulation cell at coordinate $\boldsymbol{x}$ is flagged as ionized if

$$\zeta_{\rm UV} f_{\rm coll}(\boldsymbol{x}, z, R, T_{\rm vir}) \geq 1 - x_e(\boldsymbol{x}, z, R), \quad (3)$$

where $\zeta_{\rm UV}$ is an ionizing efficiency parameter (here taken to be $\zeta_{\rm UV} = 30$ so that our reionization histories match the mean observed value of the Thompson scattering optical depth to the CMB; Hinshaw et al. 2013), and $f_{\rm coll}$ is the fraction of mass residing in dark matter haloes with virial temperatures greater than $T_{\rm vir}$ inside a sphere of radius R and mass $M = 4/3\pi R^3\rho$, where $\rho = \bar{\rho}[1 + \bar{\delta}_{\rm nl}]$, while x_e is the fraction of gas partially ionized by X-rays (Mesinger et al. 2013).

We compute the Wouthuysen–Field (WF; Wouthuysen 1952; Field 1958) coupling (i.e. Lyα pumping; when the Lyα background from the first stars couples the spin temperature to the gas temperature) using the Lyman resonance backgrounds from both X-ray excitation of H I, and direct stellar emission. The latter is found to dominate by two orders of magnitude for $f_{\rm X} \sim 1$. For the direct stellar emission, we assume standard Population II spectra from Barkana & Loeb (2005), and sum over the Lyman resonance backgrounds (Mesinger et al. 2011).

As reionization and WF coupling are not the focus of this work, we keep their relevant parameters fixed. Instead we focus on the XRB, responsible for heating and partially ionizing the IGM. The angle-averaged X-ray specific intensity, $J(\nu, \boldsymbol{x}, z)$, (in erg s^{-1} Hz^{-1} cm^{-2} sr^{-1}) can be computed integrating along the light cone:

$$J(\nu, \boldsymbol{x}, z) = \frac{(1+z)^3}{4\pi} \int_z^\infty \mathrm{d}z' \frac{c\mathrm{d}t}{\mathrm{d}z'} \epsilon_{h\nu}, \quad (4)$$

with the comoving specific emissivity evaluated at $\nu_e = \nu(1+z')/(1+z)$:

$$\epsilon_{h\nu}(\nu_e, \boldsymbol{x}, z') = \alpha h \frac{N_{\rm X}}{\mu m_p} \left(\frac{\nu_e}{\nu_0}\right)^{-\alpha} \times \left[\rho_{\rm crit,0}\Omega_{\rm b} f_* (1+\bar{\delta}_{\rm nl}) \frac{\mathrm{d}f_{\rm coll}}{\mathrm{d}t}\right], \quad (5)$$

where $N_{\rm X}$ is the number of X-ray photons per stellar baryon (recall $f_{\rm X} \equiv N_{\rm X}/0.1$), μm_p is the mean baryon mass, $\rho_{\rm crit,\,0}$ is the current critical density, f_* is fraction of baryons converted into stars (we take $f_* = 0.1$). The IGM ionization and heating (including adiabatic and Compton) is tracked locally, with the X-ray contribution computed from equation (4), given the appropriate energy deposition fractions (taken from Furlanetto & Stoever 2010).

Our fiducial model assumes that the 'first' galaxies formed in atomically cooled haloes (with virial temperatures $T_{\rm vir} \geq 10^4$ K),[11] though we also consider a couple of models with $T_{\rm vir} \geq 10^5$ K, corresponding to inefficient star formation in dwarf galaxies near the atomic cooling threshold.

4 RESULTS

We take as the main observable the 3D 21 cm power spectrum, defined as $P_{21}(k, z) = k^3/(2\pi^2\, V)\ \delta\bar{T}_b(z)^2\langle|\delta_{21}(\mathbf{k}, z)|^2\rangle_k$, where $\delta_{21}(\boldsymbol{x}, z) \equiv \delta T_b(\boldsymbol{x}, z)/\delta\bar{T}_b(z) - 1$. We focus on the large-scale power, specifically at $k = 0.2$ Mpc^{-1}. These scales are small enough to be relatively clean of foregrounds (Pober et al. 2013), while still large enough to achieve reasonable signal-to-noise ratio (S/N) with even first generation instruments (Mesinger et al. 2014). Our default power spectrum bin width is $d\ln k = 0.5$.

In most models, the amplitude of the large-scale 21 cm power rises and falls with three prominent peaks (e.g. Pritchard & Furlanetto 2007; Baek et al. 2010; see also Fig. 5), corresponding to (from high to low redshift): (i) WF coupling; (ii) X-ray heating; (iii) reionization. These are sourced mainly by fluctuations in the (i) WF coupling coefficient (sourced by the Lyα background); (ii) gas temperature; (iii) ionized fraction, respectively. WF coupling and reionization are most likely dominated by direct stellar emission of UV photons (McQuinn & O'Leary 2012; Mesinger et al. 2013). Hence, here we focus on the middle, 'X-ray heating' peak in 21 cm power, shortly after the X-rays from the first galaxies started heating the cosmic gas, and the spatial fluctuations in gas temperature[12] were the largest. After $T_{\rm S} \gg T_\gamma$, the 21 cm signal is no longer sensitive to the thermal state of the gas (cf. equation 2).

In Fig. 2, we show slices through the 21 cm brightness temperature maps for our fiducial model ($f_{\rm X} = 1$, $T_{\rm vir} = 10^4$ K), with the hard (soft) SED at the top (bottom). Both of the slices are taken at roughly the same redshift [$z_{\rm peak} = 16.7$ (16.3) for the top (bottom) panels], when the large-scale ($k = 0.2$ Mpc^{-1}) 21 cm power is the strongest in each model, corresponding to the X-ray heating peak. It is evident from the figure that the hard SED results in more uniform brightness temperature maps, due to the longer distances travelled by more energetic photons.

We quantify this in Fig. 3 which shows the corresponding temperature distributions. Specifically, we plot the cumulative distribution functions (CDFs) of $T_\gamma/T_{\rm S}$ (cf. equation 2) for the soft (red) and hard (blue) SEDs. The soft SED has a noticeably broader distribution of temperatures. Because heating is more patchy in this model, there are large regions distant from galaxies which are still cooling adiabatically at this epoch. Such cold gas is absent in the model with the hard SED. With the green curve we also show an extremely hard

[10] http://homepage.sns.it/mesinger/Sim.html

[11] The very first galaxies are likely hosted by smaller haloes, in which gas accretes via the molecular cooling channel (e.g., Haiman, Thoul & Loeb 1996; Abel, Bryan & Norman 2002; Bromm, Coppi & Larson 2002). However, H_2 is easily disrupted by external background radiation fields which sterilize star formation inside these 'minihaloes'. Even just the background radiation from atomically cooled haloes is enough to sterilize minihaloes already at $z \gtrsim 20$ (Holzbauer & Furlanetto 2012; McQuinn & O'Leary 2012; Fialkov et al. 2013; Dijkstra et al. 2014).

[12] In most models we consider, the spin temperature, $T_{\rm S}$, is already closely coupled to the gas kinetic temperature at the time of the peak in 21 cm power associated with heating. Hence we use the two terms interchangeably below.

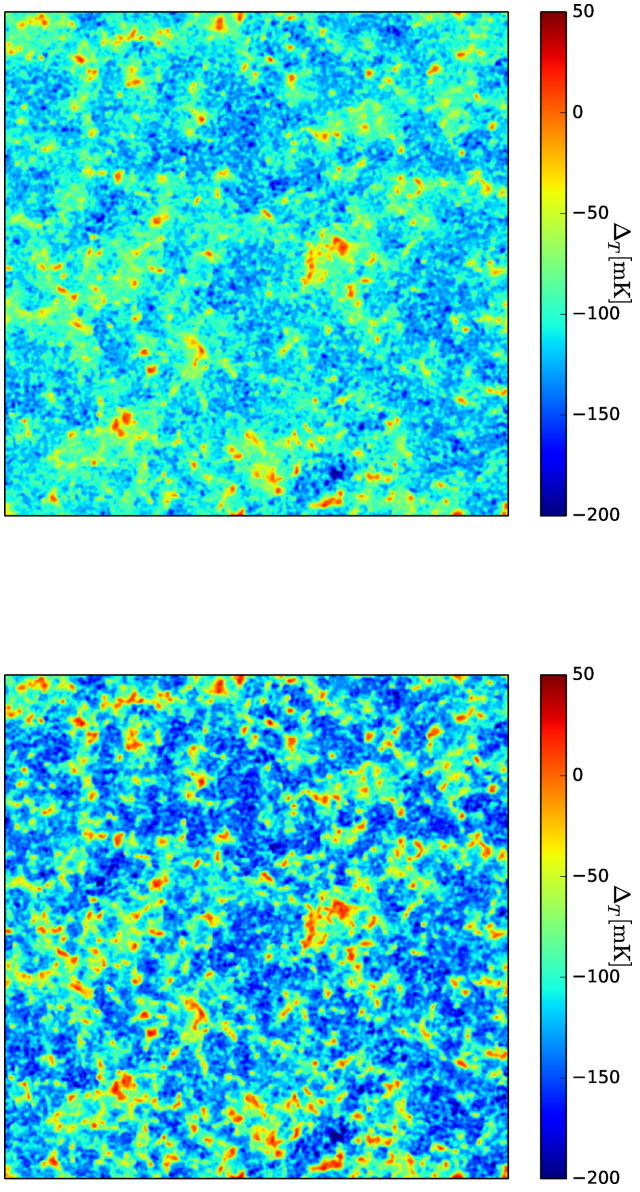

Figure 2. Slices through the 21 cm brightness temperature fields for our fiducial model with a hard (top) and soft (bottom) X-ray SED. Slices are 1.5 Mpc thick, and are taken at $z_{\rm peak} = 16.7$ (top) and $z_{\rm peak} = 16.3$ (bottom), corresponding to the redshift when the $k = 0.2$ Mpc^{-1} 21 cm power is the largest for each model.

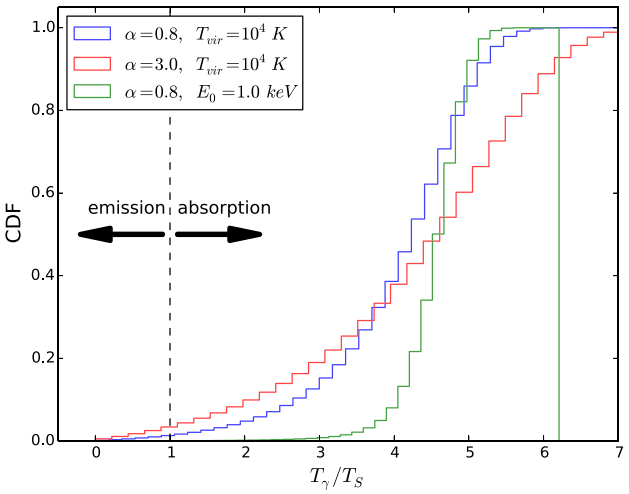

Figure 3. CDFs of $T_\gamma/T_{\rm S}$ corresponding to the fiducial soft/hard SED models shown in Fig. 2. With the green curve, we also show an extremely hard SED model, in which all soft photons with energies below $E_0 = 1$ keV are assumed to be absorbed by their host galaxies. The curves correspond to $z \sim 16.5$.

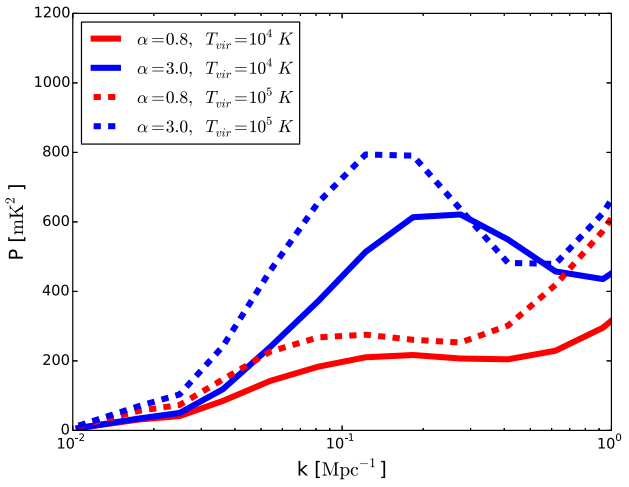

Figure 4. Power spectra corresponding to soft (blue curves) and hard (red curves) SEDs. Galaxies are assumed to be hosted by haloes with virial temperatures greater than 10^4 K (solid curves) and 10^5 K (dotted curves). As above, power spectra are taken at the redshift where the amplitude at $k = 0.2$ Mpc^{-1} is the largest, corresponding to $z_{\rm peak} \sim 16.5$ and 12, for the $T_{\rm vir} = 10^4$ and 10^5 K models, respectively.

SED model, in which all soft photons with energies below 1 keV are assumed to be absorbed by their host galaxy. With no soft photons, the heating is extremely uniform, with the temperature distribution approaching a step function.

During the X-ray heating epoch, the temperature distribution sets the 21 cm power. Broader distributions generally result in higher power spectrum amplitudes. The 21 cm power spectra corresponding to the fiducial soft/hard SED models from Fig. 2 are shown in Fig. 4. Indeed the 21 cm power is higher with the soft SED, corresponding to X-rays from the hot ISM. On large scales, this difference is a factor of ∼3. Interestingly, the power spectrum peaks at a scale of $k \sim 0.2\,{\rm Mpc}^{-1}$, which corresponds to the mean free path of the average photon in this model, $E_{\rm X} \sim 0.5$ keV. We caution however that more realistic models for the intrinsic absorption of the host galaxies could smear out this feature.

In Fig. 4, we also include power spectra for the same fiducial soft/hard SEDs, but assuming instead that the dominant galaxy population corresponds to much more massive systems, with $T_{\rm vir} \geq 10^5$ K. If such massive systems are required for efficient star formation, the X-ray heating peak is delayed until $z_{\rm peak} \sim 12$ (see Fig. 5). These host haloes are more biased than those corresponding to our fiducial, $T_{\rm vir} = 10^4$ K ones. The additional modulation by their larger correlation lengths drives the power spectrum peak to somewhat larger scales, $k \sim 0.1\,{\rm Mpc}^{-1}$. Interestingly, the large-scale power in the soft SED model is also a factor of ∼3 higher than in the hard SED model, as was the case for our fiducial choice of $T_{\rm vir}$; we elaborate more on this below.

From here on, we focus only on the amplitude of the 21 cm power at $k = 0.2$ Mpc^{-1}, lying in the narrow k-space window accessible

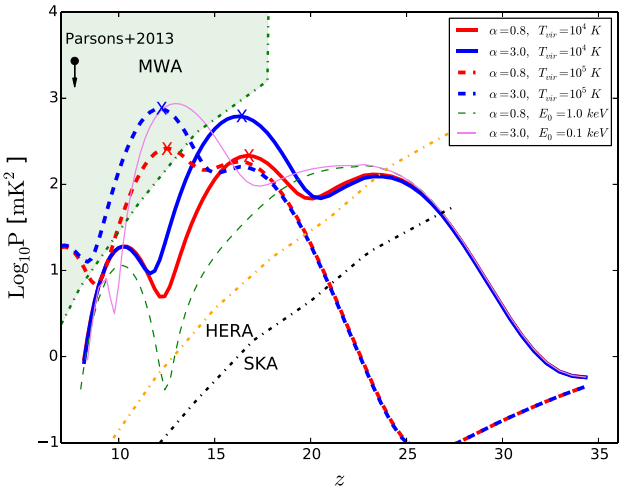

Figure 5. Redshift evolution of the 21 cm power amplitude at $k = 0.2$ Mpc^{-1}. The red and blue lines correspond to our two fiducial SEDs (soft and hard, respectively). The green (purple) line corresponds to an illustrative model with more (less) absorption by the host galaxy, such that all photons below $E_X \leq 1$ (0.1) keV are absorbed locally inside the host's ISM. The three peaks in the fiducial models correspond to (from high to low redshift): (i) WF coupling, (ii) X-ray heating (labelled with an 'X'), (iii) reionization. We also show the 2σ upper limit at $z \approx 8$ from the PAPER experiment (Parsons et al. 2013), as well as 1σ thermal noise estimates corresponding to a 1000 h observation with some upcoming and current instruments (taken from Mesinger et al. 2014).

with the first generation interferometers, as mentioned above. We note however that the evolution of large-scale power is qualitatively self-similar for a wide range of wavenumbers (e.g. Baek et al. 2010; Santos et al. 2011). In Fig. 5 we show the redshift evolution of the 21 cm power amplitude at $k = 0.2$ Mpc^{-1}. The aforementioned characteristic three-peaked structure is evident, with the WF coupling, X-ray heating and reionization peaks clearly separated in the fiducial models, assuming either $T_{\rm vir} = 10^4$ or 10^5 K. In the figure, we also present S/N estimates for three interferometric arrays: the MWA (Beardsley et al. 2012), the proposed second-generation Hydrogen Epoch of Reionization Arrays (HERA; http://reionization.org/; Pober et al., in preparation), and the SKA Phase 1 (Dewdney et al. 2013). The S/N is computed assuming a 1000 h integration, with a fixed $\Delta z = 0.5$ band. The MWA is currently taking data, and is expected to achieve 1000 h integration in $\gtrsim$2016, while HERA and the SKA are expected to begin taking observations in a few years. We note that a 1000 h survey with SKA Phase 1 is planned as part of the early science results (Koopmans et al., in preparation). For details on the noise calculations please see Mesinger et al. (2014).

Here we again see explicitly that the X-ray SED impacts the X-ray heating epoch (i.e. the middle peak). Moreover, the difference between the soft and hard SEDs is comparable (factor of $\sim$3 in power amplitude at the X-ray heating peak) for two very different choices of $T_{\rm vir}$.

In Fig. 5, we also include the redshift evolution in the $E_0 = 1$ keV model (also assuming $T_{\rm vir} = 10^4$ K, $\alpha = 0.8$, $f_X = 1$), corresponding to host-galaxy intrinsic absorption which is considerably stronger than what is observed in local galaxies. The high-energy ($\gtrsim$1 keV) X-rays which manage to escape the first galaxies in this model, heat the IGM uniformly and inefficiently (as the absorption cross-section is smaller). The uniformity of heating dramatically suppresses the temperature fluctuations (see Fig. 3), and therefore there is no noticeable X-ray heating peak (see also Mesinger et al. 2013). Furthermore, these high-energy photons interact weakly with the IGM, only managing to heat it to temperatures $T_S \sim T_\gamma$ when reionization commences. The resulting narrow temperature distribution centred around $(1 - T_\gamma/T_S) \sim 0$ (cf. equation 2) results in a much deeper drop in power at $z \sim 12$. Even at the midpoint of reionization ($z \sim 10$), the neutral IGM patches are only heated to $(1 - T_\gamma/T_S) \sim 0.6$–$0.7$, which suppresses the amplitude of the 21 cm signal by tens of per cent.

We stress that the $E_0 = 1$ keV model is quite extreme because we observe copious low-energy X-rays escaping even from nearby galaxies, which are more massive and evolved than the first galaxies. Instead, it is more likely that the first galaxies had even lower host-galaxy absorption, owing to lower average H I column densities (as discussed above). To illustrate such a scenario, we also include in Fig. 5 a model with $E_0 = 0.1$ keV, shown with a thin purple curve (also assuming $T_{\rm vir} = 10^4$ K, $\alpha = 3$, $f_X = 1$). The X-ray peak is not significantly increased in such a model, as even our fiducial hot ISM SED is soft enough to leave standing large cold patches when the IGM near the galaxies is heated (see Fig. 3). However, the peak location is shifted to lower redshifts, since the mean energy absorbed by the IGM is considerably lower in this model.

4.1 Is the imprint of the SED degenerate with the luminosity?

We noted above that the difference in the amplitude of the X-ray heating peaks for soft versus hard SEDs was remarkably similar even assuming very disparate values of $T_{\rm vir}$. In Fig. 6 we further investigate the robustness of the SED imprint by plotting the peak amplitude of the $k = 0.2$ Mpc^{-1} 21 cm power, as a function of f_X. We remind the reader that f_X is a proxy for the total number of X-ray photons per stellar baryon, serving to normalize our SEDs.

We explore a wide range of values: $10^{-2} < f_X < 10^2$. *For a given SED*, the amplitude of the peak power is remarkably constant over a wide range of luminosities: $10^{-1.5} \lesssim f_X \lesssim 10^{1.5}$, as already noted in Mesinger et al. (2014). This is due to the fact that the large-scale 21 cm power peaks when the large-scale temperature fluctuations are maximized, which is roughly a self-similar process occurring at $\delta\bar{T}_b \sim -100$ mK (Mesinger et al. 2014). If $f_X \lesssim 10^{-1.5}$, the first

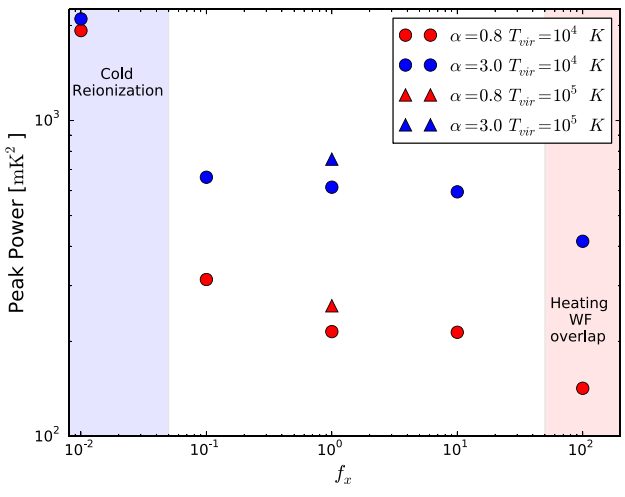

Figure 6. Peak amplitude (over all redshifts) of the $k = 0.2$ Mpc^{-1} 21 cm power, as a function of f_X. The circles (triangles) correspond to models with $T_{\rm vir} = 10^4$ (10^5) K. Red (blue) colours indicate hard (soft) SEDs. The regions of parameter space in which the X-ray heating epoch overlaps with reionization and WF coupling are shaded in blue and pink, respectively.

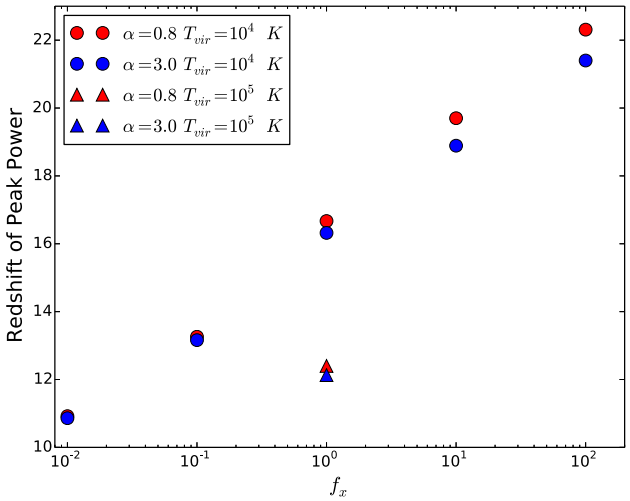

Figure 7. Same as Fig. 6, but instead showing the redshift at which the $k = 0.2$ Mpc^{-1} 21 cm power peaks on the y-axis.

galaxies are too faint in X-rays to heat the IGM before reionization commences. The resulting contrast between the ionized and very cold neutral patches can drive up the 21 cm signal considerably (e.g. Parsons et al. 2013). On the other hand if $f_X \gtrsim 10^{1.5}$, X-ray heating merges with WF coupling, and the spin temperature is never able to fully couple to the kinetic temperature, T_K, before the gas was heated. If $T_S > T_K$ during the X-ray heating peak, the amplitude of the signal decreases.

On the other hand, the amplitude of the peak power *is* strongly affected by the assumed SED. For our soft SED, corresponding to the hot ISM, the 21 cm signal peaks at $P_{21} \sim 600$–700 mK^2 over a broad range of f_X and T_{vir} values. Similarly, for our hard SED, corresponding to HMXBs, the 21 cm signal peaks at $P_{21} \sim 200$–300 mK^2, again over a broad range: $10^{-1.5} \lesssim f_X \lesssim 10^{1.5}$ and 10^4 K $\lesssim T_{vir} \lesssim 10^5$ K. Therefore, *the peak amplitude of the large-scale 21 cm power is a robust probe of the X-ray SED of the first galaxies*, not degenerate with their X-ray luminosities and host halo masses.

Finally, Fig. 7 shows the redshift of the peak power, z_{peak}, on the vertical axis, as a function of the X-ray efficiency f_X. An increase in the X-ray efficiency, or a decrease in the host halo virial temperature, corresponds to a higher z_{peak}, since the IGM is heated earlier. However, the X-ray SED does not have a strong impact on the redshift of the peak power.

Thus, upcoming interferometers can determine the X-ray luminosities and host halo mass of the first galaxies from the redshift of the peak 21 cm power (Mesinger et al. 2014), while the *amplitude of the peak power can constrain the SED*. Hence we should soon have a complete picture of the X-ray properties of the first galaxies.

5 CONCLUSIONS

In this proof-of-concept, we investigated if the X-ray SED of the first galaxies could have a robust imprint in the 21 cm signal. We were motivated by *Chandra* observations of local star-forming galaxies, in which the relevant soft-band luminosity has two main contributors: (i) the hot, diffuse ISM and (ii) HMXBs. Using simple SEDs corresponding to these two populations, we studied their imprint on the 21 cm signal, focusing on the epoch when the first galaxies began heating the IGM with their X-rays.

Understandably a soft SED, representative of the hot ISM, results in larger fluctuations of the IGM temperature, as the absorption cross-section for X-rays has a strong dependence on the photon energy. Low-energy photons are much more likely to be absorbed closer to the galaxies. These stronger temperature fluctuations drive up the amplitude of the large-scale ($k \sim 0.2$ Mpc^{-1}) 21 cm power by a factor of ~ 3, compared with models dominated by hard SEDs representative of HMXBs.

More generally, we show that the X-ray SED determines the amplitude of the peak 21 cm power, for a wide range of X-ray luminosities ($10^{-1.5} \lesssim f_X \lesssim 10^{1.5}$) and host halo virial temperatures (10^4 K $\lesssim T_{vir} \lesssim 10^5$ K). The reverse is true for the redshift at which the large-scale power peaks: it is insensitive to the SED, and instead determined by the X-ray luminosity and host halo mass of the first galaxies. Thus, upcoming interferometers can determine the X-ray luminosities and host halo mass of the first galaxies from the redshift of the peak 21 cm power, while the amplitude of the peak power will constrain the SED.

The absorption intrinsic to the host galaxies remains a significant source of uncertainty, and could substantially impact the emerging soft-band SED. In this work, our fiducial models assume a sharp cut below $E_0 = 0.3$ keV, corresponding to photons whose mean free path is greater than unity given the same column densities observed in local galaxies, *but* assuming a low metallicity such that the ISM absorption is dominated by hydrogen and helium. If on the other hand the emerging X-ray SED of the first galaxies is *exactly* as observed in local ones, the 21 cm signal should be as predicted in our hard, $\alpha = 0.8$ models. This is because in observed composite spectra (see Fig. 1), the additional absorption of the HMXB template at $\lesssim$1 keV provided by the metals is almost exactly compensated for by the additional contribution from the absorbed, hot ISM. This makes the total spectrum (absorbed hot ISM + absorbed HMXBs) look like an unabsorbed, $\alpha \sim 0.8$ power law down to low energies ($\lesssim$0.5 keV), which is effectively our hard SED for the first galaxies.

Subsequent work will focus on constructing more complete and detailed models of the X-ray SEDs emerging from the first galaxies, guided by hydrodynamic simulations including metal pollution. Combined with upcoming 21 cm interferometric observations, we will be able to robustly study high-energy processes inside the first galaxies.

ACKNOWLEDGEMENTS

We thank Bret Lehmer for stimulating conversations which contributed to motivating this work. SM acknowledges support from the NASA's Astrophysics Data Analysis Program (ADAP) grant NNH13CH56C.

REFERENCES

Abel T., Bryan G. L., Norman M. L., 2002, Science, 295, 93
Alvarez M. A., Finlator K., Trenti M., 2012, ApJ, 759, L38
Bachetti M. et al., 2013, ApJ, 778, 163
Baek S., Semelin B., Di Matteo P., Revaz Y., Combes F., 2010, A&A, 523, A4
Barkana R., Loeb A., 2005, ApJ, 626, 1
Basu-Zych A. R. et al., 2013, ApJ, 762, 45
Beardsley A. P. et al., 2012, MNRAS, 425, 1781
Brandt W. N., Comastri A., Gallagher S. C., Sambruna R. M., Boller T., Laor A., 1999, ApJ, 525, L69
Bromm V., Coppi P. S., Larson R. B., 2002, ApJ, 564, 23
Christian P., Loeb A., 2013, JCAP, 9, 14
Dewdney P. et al., 2013, SKA1 System Baseline Design, available at: http://www.skatelescope.org/wp-content/uploads/; 2013/03/SKA-TEL-SKO-DD-001-1_BaselineDesign1.pdf, p. 1

Dijkstra M. et al., 2014, MNRAS, 442, 2036
Fan X. et al., 1999, ApJ, 526, L57
Ferrara A., Loeb A., 2012, MNRAS, 431, 2826
Fialkov A., Barkana R., Visbal E., Tseliakhovich D., Hirata C. M., 2013, MNRAS, 432, 2909
Fialkov A., Barkana R., Visbal E., 2014, Nature, 506, 197
Field G. B., 1958, Proc. Inst. Radio Eng., 46, 240
Fragos T., Lehmer B. D., Naoz S., Zezas A., Basu-Zych A., 2013, ApJ, 776, L31
Furlanetto S. R., 2006, MNRAS, 371, 867
Furlanetto S. R., Stoever S. J., 2010, MNRAS, 404, 1869
Furlanetto S. R., Zaldarriaga M., Hernquist L., 2004, ApJ, 613, 1
Furlanetto S. R., Oh S. P., Briggs F. H., 2006, Physics Reports, 433, 181
Gaetz T. J., Salpeter E. E., 1983, ApJS, 52, 155
Gilfanov M., 2010, in Belloni T., ed., Lecture Notes in Physics, Vol. 794, X-Ray Emission from Black-Hole Binaries. Springer-Verlag, Berlin, p. 17
Gilfanov M., Grimm H.-J., Sunyaev R., 2004, MNRAS, 347, L57
Grimes J. P., Heckman T., Strickland D., Ptak A., 2005, ApJ, 628, 187
Grimm H.-J., Gilfanov M., Sunyaev R., 2003, MNRAS, 339, 793
Haardt F., Madau P., 2012, ApJ, 746, 125
Haiman Z., Thoul A. A., Loeb A., 1996, ApJ, 464, 523
Hinshaw G. et al., 2013, ApJS, 208, 19
Holzbauer L. N., Furlanetto S. R., 2012, MNRAS, 419, 718
Kaaret P., 2014, MNRAS, 440, L26
Kuhlen M., Faucher-Giguere C.-A., 2012, MNRAS, 423, 862
Lehmer B. D., Alexander D. M., Bauer F. E., Brandt W. N., Goulding A. D., Jenkins L. P., Ptak A., Roberts T. P., 2010, ApJ, 724, 559
Li J.-T., Wang Q. D., 2013, MNRAS, 435, 3071
McClintock J. E., Remillard R. A., 2006, Cambridge Astrophysics Series No. 39, Black Hole Binaries. Cambridge Univ. Press, Cambridge, p. 157
McQuinn M., 2012, MNRAS, 426, 1349
McQuinn M., O'Leary R. M., 2012, ApJ, 760, 3
Mellema G. et al., 2013, Exp. Astron., 36, 235
Mesinger A., Furlanetto S., 2007, ApJ, 669, 663
Mesinger A., Furlanetto S., Cen R., 2011, MNRAS, 411, 955
Mesinger A., Ferrara A., Spiegel D. S., 2013, MNRAS, 431, 621
Mesinger A., Ewall-Wice A., Hewitt J., 2014, MNRAS, 439, 3262
Mineo S., Gilfanov M., Sunyaev R., 2012a, MNRAS, 419, 2095
Mineo S., Gilfanov M., Sunyaev R., 2012b, MNRAS, 426, 1870
Mirabel I. F., Dijkstra M., Laurent P., Loeb A., Pritchard J. R., 2011, A&A, 528, A149
Miyawaki R., Makishima K., Yamada S., Gandhi P., Mizuno T., Kubota A., Tsuru T. G., Matsumoto H., 2009, PASJ, 61, 263
Moretti A., Vattakunnel S., Tozzi P., Salvaterra R., Severgnini P., Fugazza D., Haardt F., Gilli R., 2012, A&A, 548, A87
Morrison R., McCammon D., 1983, ApJ, 270, 119
Owen R. A., Warwick R. S., 2009, MNRAS, 394, 1741
Parsons A. R. et al., 2010, AJ, 139, 1468
Parsons A. R. et al., 2013, ApJ, 788, 106
Persic M., Rephaeli Y., 2007, A&A, 463, 481
Planck Collaboration, 2013, preprint (arXiv:1303.5076)
Pober J. C. et al., 2013, ApJ, 768, L36
Pritchard J. R., Furlanetto S. R., 2007, MNRAS, 376, 1680
Ranalli P., Comastri A., Setti G., 2003, A&A, 399, 39
Rephaeli Y., Gruber D., Persic M., 1995, A&A, 300, 91
Santos M. G., Silva M. B., Pritchard J. R., Cen R., Cooray A., 2011, A&A, 527, A93
Shakura N. I., Sunyaev R. A., 1973, A&A, 24, 337
Strickland D. K., Heckman T. M., Weaver K. A., Dahlem M., 2000, AJ, 120, 2965
Strickland D. K., Heckman T. M., Colbert E. J. M., Hoopes C. G., Weaver K. A., 2004, ApJS, 151, 193
Swartz D. A., Ghosh K. K., Tennant A. F., Wu K., 2004, ApJS, 154, 519
Swartz D. A., Soria R., Tennant A. F., Yukita M., 2011, ApJ, 741, 49
Tingay S. J. et al., 2013, Publ. Astron. Soc. Aust., 30, 7
Valdés M., Evoli C., Mesinger A., Ferrara A., Yoshida N., 2013, MNRAS, 429, 1705
van Haarlem M. P. et al., 2013, A&A, 556, A2
Walton D. J., Roberts T. P., Mateos S., Heard V., 2011, MNRAS, 416, 1844
Wise J. H., Abel T., Turk M. J., Norman M. L., Smith B. D., 2012, MNRAS, 427, 311
Wouthuysen S. A., 1952, AJ, 57, 31
Zahn O., Mesinger A., McQuinn M., Trac H., Cen R., Hernquist L. E., 2011, MNRAS, 414, 727
Zel'Dovich Y. B., 1970, A&A, 5, 84

This paper has been typeset from a TEX/LATEX file prepared by the author.